Modeling of Synchronized Bursting Events: The Importance of Inhomogeneity

Erez Persi*, David Horn, Vladislav Volman, Ronen Segev and Eshel Ben-Jacob

School of Physics and Astronomy

Raymond & Beverly Sackler Faculty of Exact Sciences

Tel-Aviv University, Tel-Aviv 69978, Israel

May 14, 2004

*communicating author, presently at Laboratoire de Neurophysique et Physiologie du system moteur, CNRS UMR 8119, 75270 Paris cedex 06, France, email: erez.persi@biomedicale.univ-paris5.fr, telephone no.: +33-1-42863358

Abstract

Cultured *in vitro* neuronal networks are known to exhibit synchronized bursting events (SBE), during which most of the neurons in the system spike within a time window of approximately 100msec. Such phenomena can be obtained in model networks based on Markram-Tsodyks frequency-dependent synapses. We point out that in order to account correctly for the detailed behavior of SBEs, several modifications have to be implemented in such models. Random input currents have to be introduced to account for the rising profile of SBEs. Dynamic thresholds and inhomogeneity in the distribution of neuronal resistances enable us to describe the profile of activity within the SBE and the heavy-tailed distributions of inter-spike-intervals and inter-event-intervals. Thus we can account for the interesting appearance of Lévy distributions in the data.

Key words: Synchronized bursts; Dynamic synapses; Lévy distribution; ISI; IEI.

1 Introduction

How an ensemble of neurons links together to form a functional unit is a fundamental problem in neuroscience. The difficulty in visualizing and measuring the activity of *in vivo* neuronal networks has accelerated the tendency to pursue surrogate methods. As a result, much effort has been devoted to studying cultured neuronal networks *in vitro*. It has been suggested (Marom & Shahaf, 2002; Shahaf & Marom, 2001) that large random networks *in vitro* are probably the most appropriate experimental model to study the formation of activity of groups of neurons, and the response of this functional connectivity to stimulation. Unlike *in vivo* networks, randomly formed *in vitro* networks are free of any predefined functional role, and enable one to study how a system self-organizes.

Many different forms of synchronized activity of populations of neurons have been observed in the central nervous system (CNS) throughout the years. However, the role of synchronization in the neural code and information processing is still a matter of considerable debate. Recently Segev et al. (Segev et al., 2001a; Segev et al., 2001b) performed long-term measurements of spontaneous activity of *in vitro* neuronal networks placed on multi-electrode arrays. These developing networks show interesting temporal and spatio-temporal properties on many time scales. At early stages (up to a week) the neurons spike sporadically, after which they begin to correlate, leading to the emergence of synchronized bursting events (SBEs). A SBE involves extensive spiking of a large fraction of neurons in the system during approximately 100msec. One hypothesis (Segev, 2002) is that these dynamical SBEs are the substrate for information encoding at the network level, in analogy with action potentials at the neuronal level.

Different morphological structures and sizes of networks were explored

(Segev et al., 2001a). All networks exhibit: 1. Long-term correlation of the SBEs' time sequence manifested by power-law decay of the power-spectrum density. 2. Temporal-scaling behavior of neuronal activity during the SBEs (where most of the activity takes place). 3. Temporal-scaling behavior of the SBEs' time sequence. Temporal-scaling is usually expressed by a power-law decay. The time sequences of spikes and SBEs were well-fitted to a Lévy distribution, that has a power-law decay. Such scale-invariant behavior is characteristic of dynamical systems which are composed of many non-linear components (Mantegna & Stanley, 1995; Peng et al., 1993).

Our goal is to elucidate the underling mechanisms and properties of the different elements in the system, that are responsible for the generation and structure of the observed neuronal (synchronized) activity.

2 Experimental Observations

The experimental system is based on a two-dimensional (2D) 60 multi-electrode array on which the biological system is grown. The biological system is composed of both neurons and glia, taken from the cortex of a baby rat. The coupling between the electrodes and the neuronal membranes enables the recording of neuronal electric activity (action potentials). Different morphological types and sizes of networks were explored (Segev et al., 2001a): 1. quasi one-dimensional (1DS) - a small network composed of 50 cells. 2. rectangular (2DM) - a medium-sized network composed of 10^4 cells. 3. circular (2DL) - a large size network composed of 10^6 cells. All these networks shared the same characteristic patterns of activity. The mean rate of SBEs increases with the size of the network, while the variance decreases but only up to a factor of 2.

2.1 Synchronized Bursting Events

Figure 1 illustrates a characteristic raster plot, revealing the appearance of SBEs and their structure. The SBE involves rapid spiking of almost all the neurons in the network. It starts abruptly and decays during a 100msec period. During the SBE each neuron has its own firing pattern, consisting of up to 20 spikes. The SBEs are separated by long quiescent periods (1-10sec) during which there is almost no activity except for few sporadic spikes. The mean rate of SBEs is between 0.1Hz and 0.4Hz.

2.2 Distribution of Neuronal Activity

The distributions of ISI at the neuron level, and inter-event interval (IEI) at the network level, were analyzed (Segev et al., 2001a). Since the SBE width is of order 100msec, this defines the resolution of IEIs. The ISI and IEI distributions of experimental data reveal heavy tails, indicating possible temporal-scaling behavior. To study the appearance of heavy tails in ISI and IEI, the distributions of the ISI and IEI increments, defined by

$$\Delta ISI(t) = ISI(t) - ISI(t-1) \tag{1}$$

$$\Delta IEI(t) = IEI(t) - IEI(t-1) \tag{2}$$

were investigated. Unlike the ISI and IEI, the increments have symmetric stationary distributions with zero mean. Figure 2 displays the histograms of the ISI increments of three different neurons, as well as the average of all experimental data and the margin of variation. We note that since the activity is very low between any two consecutive SBEs, the first part of the histogram (up to 100msec) is separated from the second part (from 2sec) which reveals the heavy-tailed distribution of the IEI increments (since ISI increments larger than 1-2sec are caused mainly by the SBEs). Between 100msec to 2sec

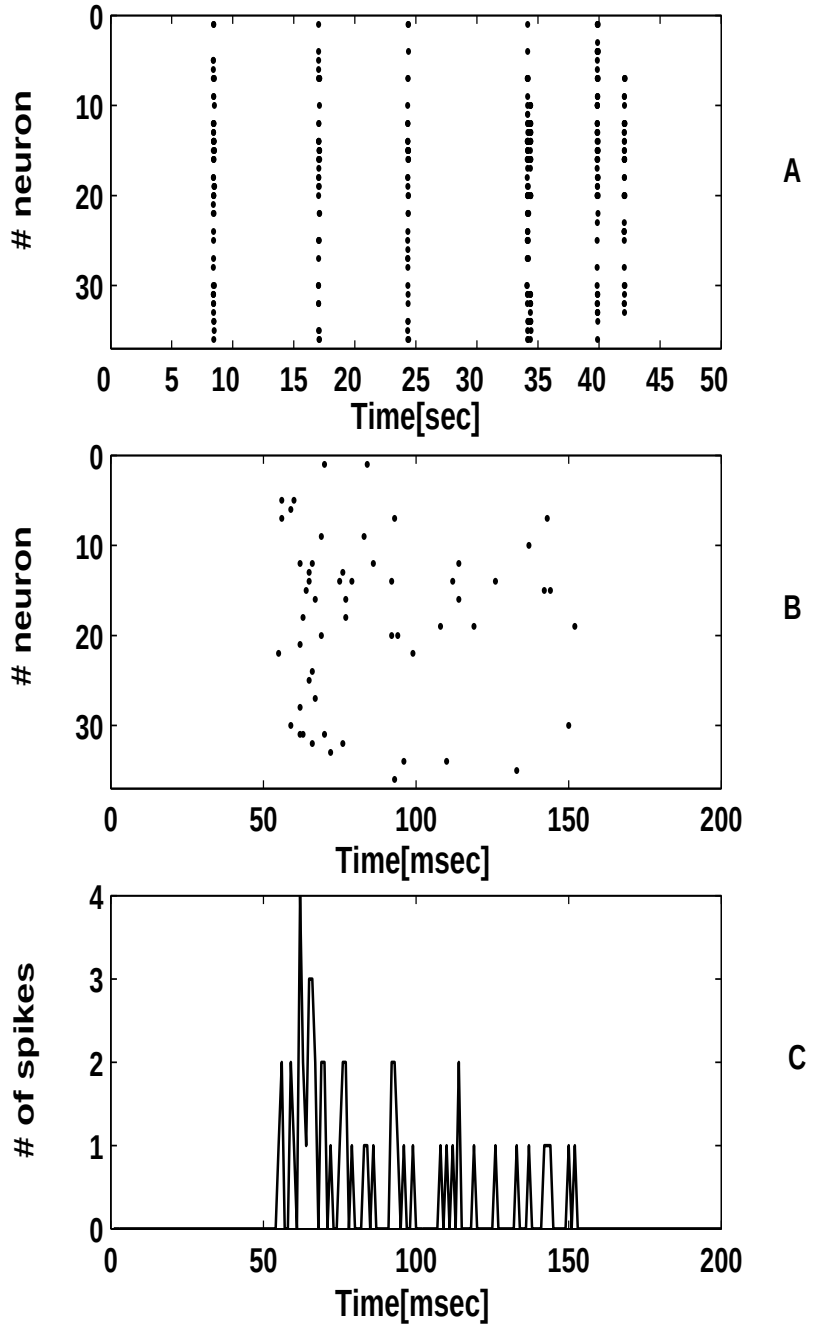

Figure 1: Typical activity of the experimental network. Upper frame: The raster plot of 1msec time-bins reveals SBEs. Middle frame: zoom into the SBEs. Lower frame: Detailed structure of a SBE, displayed by the number of spikes in the network per time-bin.

the probability increases slightly for each neuron due to both the synchrony and sporadic activity in the system. We also calculate the distance between the individual neurons' histograms and the averaged histogram using the KL divergence measure defined by:

$$D_{KL} = \sum_x P(x) \cdot log_2(P(x)/Q(x)) \tag{3}$$

The values are given in the figure caption. These values will be compared later with model neurons.

Since these distributions exhibit large tails it seems only natural to try and fit them by Lévy distributions, which would also be expected from central limit theorem arguments (see below). In this paper we follow the parameterization $S(\alpha, \beta, \gamma, \delta; 0)$ (Nolan, 1998; Nolan, 2004) to describe Lévy distribution.

Every Lévy distribution is a stable distribution. A random variable X is stable if $X_1 + X_2 + \cdots + X_n \sim C_n X + D_n$, meaning that the normalized sum of independent and identically distributed (iid) random variables is also distributed as X, with a scaling factor $C_n = n^{1/\alpha}$, and a shift D_n. For the data in Figure 2 we find that ΔISI distributions are well-fitted with a Lévy distribution $S(\alpha, 0, \gamma, 0; 0)$ up to 100msec, while ΔIEIs are well-fitted with Lévy over another 3 decades. $0 < \alpha \leq 2$ is the index of stability, which determines the long tail of the distribution, and $\gamma > 0$ is a scale factor, which determines the location of the bending point (see examples in Figure 3). Special cases of the Lévy distributions are the Gaussian distribution ($\alpha = 2$) and the Cauchy distribution ($\alpha = 1$). All $\alpha < 2$ have divergent variance.

There are several important properties of Lévy distributions worth pointing out: 1. The generalized central limit theorem (Nolan, 2004) states that the normalized sum of iid variables converges to a Lévy distribution. If the variance is finite then $\alpha = 2$, i.e., the convergence is to a Gaussian distribution. Otherwise, $\alpha < 2$. 2. If $\alpha < 1$ the mean is infinite too. 3. For $\alpha < 2$ the asymptotic

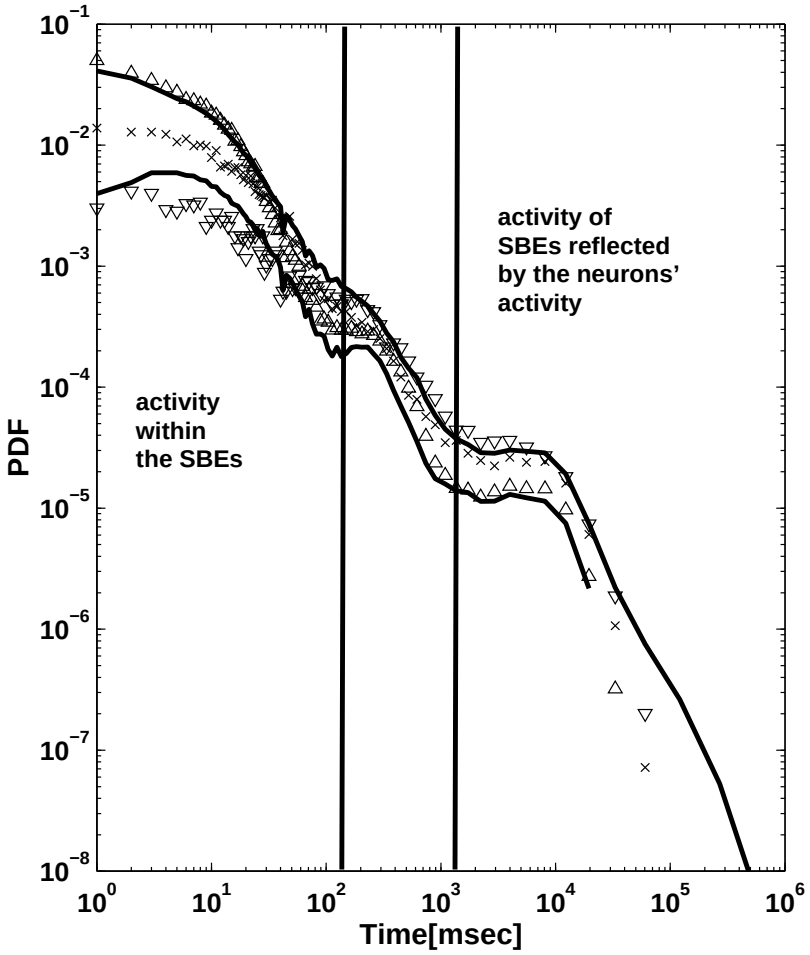

Figure 2: Positive-half of the neurons' ΔISI histograms, taken from the experimental data. Solid lines represent the margins of variability. They are calculated by averaging the histograms of all neurons and plotting this averaged PDF $\pm$ the standard deviation. Symbols represent data of 3 selected neurons, also showing the diversity in the data. The KL-distance measures of these neurons from the average PDF are $4.1193 \cdot 10^{-6}$, $3.1369 \cdot 10^{-6}$, $3.1355 \cdot 10^{-5}$ ordered according to the order of the neuron values at Time=1 from top to bottom.

behavior of the distribution is given by a power law $f(\mid X \mid) \propto \mid X \mid^{-(1+\alpha)}$.

In Figure 3 we present examples of different Lévy distributions plotted on log-log scales of the type used in Figure 2. This should help developing the understanding that γ replaces the SD parameter, specifying when the bending of the PDF occurs on the log-log plot. α determines the slope of the long tail. Since there are no closed forms for these stable distributions (except for particular cases), we use numerical simulations and display histograms instead of analytic distribution functions.

The observed behavior of ΔISI and ΔIEI implies that their variances diverge, i.e. that there is no characteristic time scale in the system. Previous models of IF neurons with dynamic synapses were unable to account for these heavy-tailed distributions (Segev et al., 2001a). Our aim is to suggest mechanisms that will generate distributions of the kind observed experimentally.

3 The Model

Our model is based on leaky integrate and fire (IF) neurons endowed with frequency-dependent synapses (Markram & Tsodyks, 1996). An IF neuron captures the most important aspects of neuronal behavior: the integration of inputs during the sub-threshold period and the generation of a spike once the threshold is reached. The IF neuron is described by

$$\tau_{mem} \cdot \frac{dv}{dt} = -v + R_{mem} \cdot (I_{syn} + I_{ext}) \tag{4}$$

where v, τ_{mem} and R_{mem} are the voltage, time constant and resistance of the cell membrane, respectively. Once v reaches a threshold the neuron fires and v is being reset to v_{res}.

Neural networks composed of IF neurons are able to generate bursting activity (Tsodyks, Uziel & Markram, 1999) in a model based on frequency-

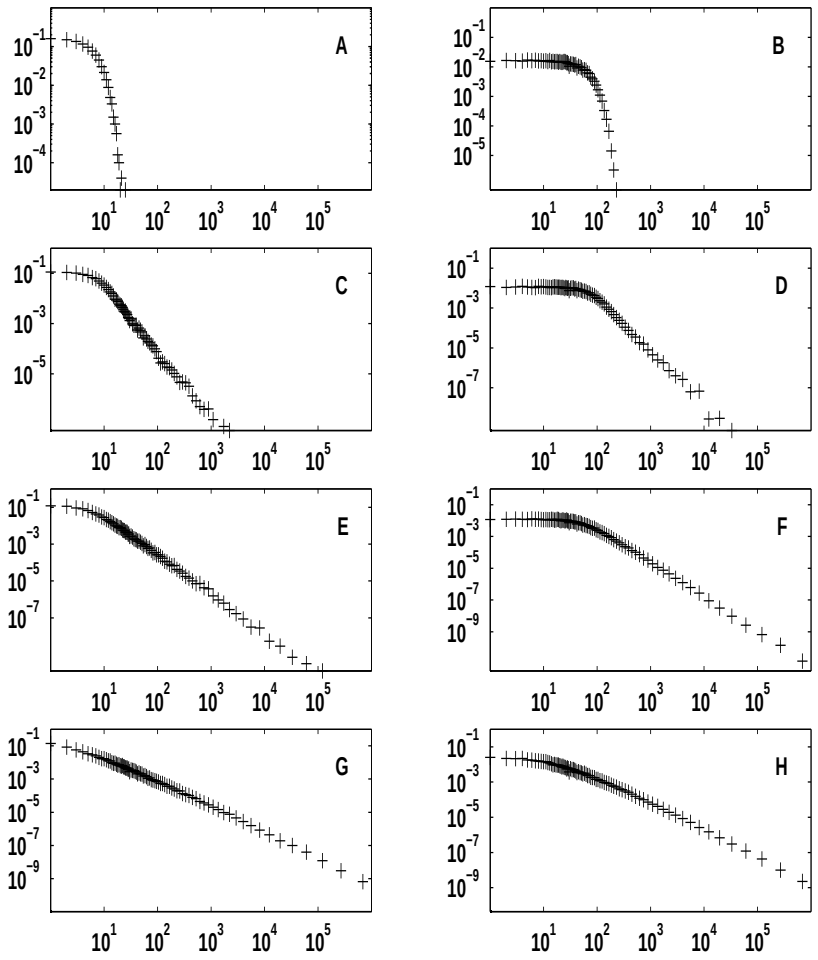

Figure 3: Examples of the positive half of Gaussian and Lévy distributions on logarithmic scale. First row: Gaussian distributions with SD=5 (left) and SD=50 (right). Notice that increasing the variance shifts the bending point to the right but does not affect the asymptotic behaviour of the distribution. Second row: Lévy distributions with $\alpha = 1.5$, $\gamma = 5$ (left) and $\gamma = 50$ (right). Notice the slow convergence to zero of the tails. Third row: Lévy distributions with $\alpha = 1.05$, $\gamma = 5$ (left) and $\gamma = 50$ (right). Fourth row: Lévy distributions with $\alpha = 0.5$, $\gamma = 5$ (left) and $\gamma = 50$ (right).

dependent synapses. The phenomenological model of dynamic synapses was shown to accurately predict the behavior and properties of various neocortical connections (Markram et al., 1998; Tsodyks Pawelzik & Markram, 1998). The strength of a synapse is described by a parameter A_{ij}, representing the efficacy of a synapse connecting a pre-synaptic neuron (j) to a post-synaptic neuron (i). The dynamics of the synapse is described by the following system of differential equations:

$$\frac{dx}{dt} = \frac{z}{\tau_{rec}} - u \cdot x \cdot \delta(t - t_{sp}) \tag{5}$$

$$\frac{dy}{dt} = -\frac{y}{\tau_{ina}} + u \cdot x \cdot \delta(t - t_{sp}) \tag{6}$$

$$\frac{dz}{dt} = \frac{y}{\tau_{ina}} - \frac{z}{\tau_{rec}} \tag{7}$$

where x, y, z are state variables representing the fraction of ionic channels in the synapse in the recover, active and inactive states, respectively, with $x + y + z = 1$. u represents the fraction of utilization of the recover state by each pre-synaptic spike. Once a spike from a pre-synaptic neuron arrives at the synaptic terminal at time t_{sp}, a fraction u of the recover state is transferred to the active state, which represents the fraction of open ionic channels through which neurotransmitters can flow. The synaptic current from all pre-synaptic neurons to the post-synaptic neuron is therefore:

$$I^i_{syn} = \sum_{j=1}^{n} A_{ij} \cdot y_{ij} \tag{8}$$

After a short time τ_{ina} the ionic channels switch into the inactive state. From the inactive state there is a slow process of recovery ($\tau_{rec} >> \tau_{ina}$) back to the recover state, completing a cycle of synapse dynamics. The above description (with a constant variable u) captures well the dynamics of a depressing synapse. The variable u describes the effective use of synaptic resources and could be assigned to the probability of release of neurotransmitters. In facilitating synapses, each pre-synaptic spike increases the probability to excrete

neurotransmitters to the synaptic cleft. In order to also capture the dynamics of facilitating synapses, another equation was added to the model:

$$\frac{du}{dt} = -\frac{u}{\tau_{fac}} + U \cdot (1-u) \cdot \delta(t - t_{sp}) \tag{9}$$

where the constant parameter U determines the increase in the value of u each time a pre-synaptic spike arrives. The initial condition is that $U = u$. Note that when τ_{fac} approaches zero facilitation is not exhibited. When a pre-synaptic spike arrives, u is updated first, and then all other parameters *(x, y, z)*.

Tsodyks et al. (Tsodyks, Uziel & Markram, 1999) have demonstrated that a network of IF neurons with dynamic synapses of the type described above generates synchronized bursts. Their network was composed of 400 excitatory neurons and 100 inhibitory neurons with probability of 0.1 for connection between two neurons. Each post-synaptic excitatory neuron is connected to a pre-synaptic neuron through a depressing synapse, while each post-synaptic inhibitory neuron is connected through a facilitating synapse. The network is partially balanced, i.e. on average $3 \cdot A_{EE} = A_{EI}$, but $A_{IE} = A_{II}$. The network was fed a fixed external input current I_{ext} which was generated by a random flat distribution centered at firing threshold (with a range of 5% of the threshold). The rate of SBEs obtained with this description is approximately 1Hz. After a SBE occurs it fades away rapidly since the fast firing neurons with depressing connections cause a sharp decline of recovering synapses. Between SBEs there is a low-rate activity which enables the recovery of synapses, so I_{syn} builds up and leads to a new burst. Choice of parameters is given in the Appendix.

Trying this approach on our system we find that it needs modifications. It is difficult to find parameters that fit both the rate of SBEs and the low firing rate of neurons in between SBEs. Moreover, the profile of the experimental SBE, i.e. the activity of neurons within this event, rises sharply and decays

exponentially, while the model as described so far leads to a narrow (20msec) Gaussian profile. The modifications that we propose are discussed in the next section.

4 Importance of Noise, Inhomogeneity and Dynamic Thresholds

Here we investigate three modifications of the model described above. We add noise to the input current, we introduce inhomogeneity into the resistances, and add dynamic thresholds which are also inhomogeneously distributed. The simulations reported below were performed on a network of 27 excitatory and 3 inhibitory neurons with 25% connectivity. For simplicity we chose V_{th} and V_{res} to be 1 and 0 respectively and $\tau_{mem} = 10$msec. Since τ_{ina} determines the decay of synaptic currents which dominate during the SBE, we increased τ_{ina} to 10msec. This leads to wide bursts of order 100msec.

The biological system is grown on top of a biochemical substrate. Therefore, the neurons in the dish are subjected to sustained changes in the concentration of different substances which compose the external environment of the neurons. For more details on the experimental methods see (Segev 2002; Segev et al., 2001b). In addition, each neuron (in the large networks) receives thousands of noisy synaptic inputs. We introduce external noisy current in our model in order to account for all these effects, as well as other hidden biological mechanisms, both on the neuronal and the synaptic levels. The external noise is chosen to be Gaussian with expectation value of $\mu = 0.86$ and standard deviation of $\sigma = 0.15$. Each 10 time steps (of 0.1msec each) a different value of the external current is used. This leads to both quiescence between successive SBEs, and to sharp increase in neuronal activity once a SBE starts, as shown in

Figure 4. Since μ is below threshold, the neurons' firing rate is very low. This enables the synapses to recover quickly and almost completely before the next SBE. At the point where the synapses are recovered, a single spike from one of the neurons in the network generates a large I_{syn} in its targets, thus increasing the probability to generate a SBE. When the SBE fades away the synapses are in the inactive state, hence the only activity is the one driven by the noisy external currents. The expectation value and variance of the noise control the mean rate of SBEs, that can be adjusted to fit the experimental values. However, the profile of the simulated SBE builds up too fast in comparison with experiments. The ΔISI distribution possesses a heavy tail (power-law behavior up to 100msec), but it does not fit a Lévy distribution. This is a direct result of high activity during the SBE, since the probability for large ΔISI during the SBE is too low.

To cure these problems we introduce inhomogeneity into the system. We start with inhomogeneity in neuronal resistances, the R_{mem} parameters of Eq. 3. We select them randomly from a flat distribution over the interval [0.1, 0.4]. This modifies each neuronal I_{syn}, and the correlations between the activity of neurons during the SBE are weakened leading to a slower SBE build up. Since $I_{syn} \sim A_{ij}$ this is actually a rescaling of synaptic strengths. The resulting SBE matches perfectly the observed spatio-temporal structure (see Figure 5). Moreover, this choice leads to a Lévy distribution in ΔISI up to 50msec, which suggests that the system still lacks a mechanism that allows the probability for large ΔISI to increase.

Next we introduce dynamic thresholds, in order to improve the Lévy distributions of ΔISI and ΔIEI. Adaptation and regulation are well-known characteristics of neuronal activity. It may be represented by dynamical thresholds, allowing for fatigue to set in upon receiving strong stimulation over long pe-

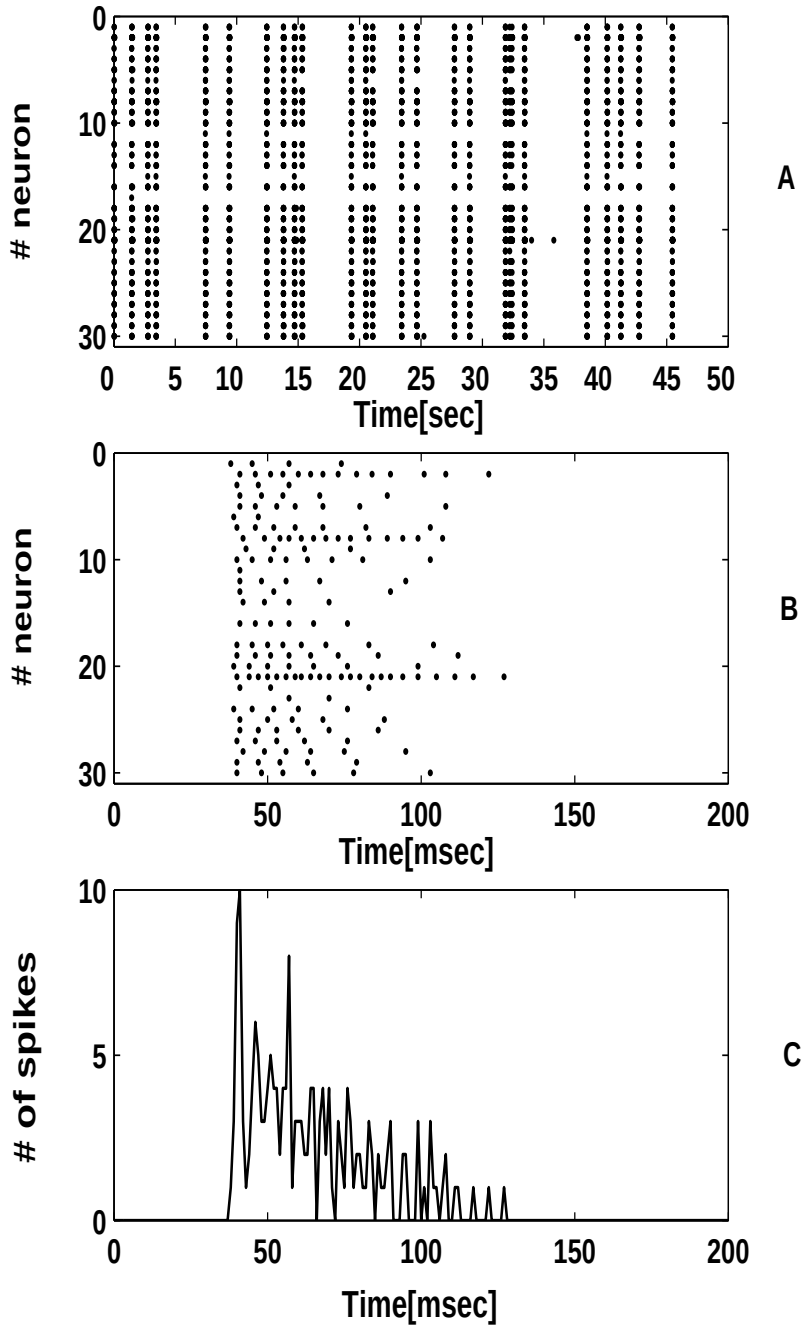

Figure 4: The bursting profile due to noisy external currents. Top: raster plot shows the quiescence between SBE. Middle: zoom into the SBE at 20sec. The SBE width is 100msec. Bottom: the activity during SBE has the right profile but is too intensive.

riods. For recent discussions of these effects see (Horn & Usher, 1989; Horn & Opher, 1999; Ying & Wang, 2000; Brandman & Nelson, 2002). Here we introduce dynamic thresholds that change as function of the neuronal firing rate:

$$\frac{d\theta_i}{dt} = -\frac{\theta_i - \theta_i(t=0)}{\tau_{th}} + \eta_i \cdot \delta(t - t_{sp}) \tag{10}$$

θ describes the change in threshold, η_i is a factor chosen from a flat distribution over the interval [-0.05,+0.05], and τ_{th} equals the SBE time width (100msec), consistent with biological data. Note that our choices for η_i mean that there are two kinds of neurons, with thresholds that increase or decrease during an SBE. In other words, one kind of neurons displays fatigue while the other displays facilitation. Using this description we obtain a good match (over five decades) to the probability distribution functions of ΔISI and ΔIEI, and to the experimental spatio-temporal structure of SBEs, as demonstrated in Fig. 5, 6.

The fit to ΔIEI is interesting. Note that with homogeneous synaptic strengths, refractory periods, membrane time constant etc., the probability to generate a SBE is determined by the time-varying external inputs and by the specific connectivity of the network. This leads to a periodic-like SBE behavior as in Tsodyks et al. (Tsodyks, Uziel & Markram, 1999). By allowing slight dynamical changes in these parameters, we are able to generate aperiodic behavior with long periods of quiescence, resulting in a Lévy distribution. The choice of parameters is given in the Appendix. Also τ_{mem} and τ_{ref} are selected from a flat distribution. This enables us to limit the dispersion of the selected values of the resistances, but is not crucial to obtain the effects we discussed above.

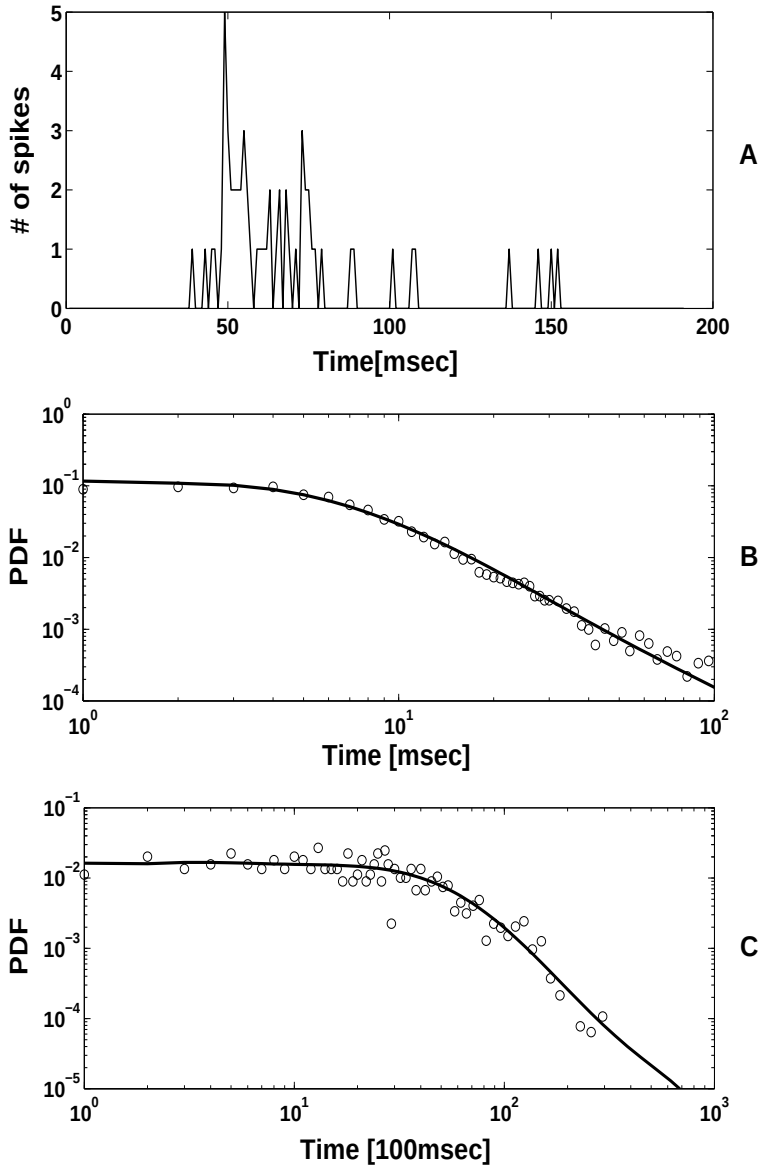

Figure 5: Effect of dynamic thresholds and inhomogeneous resistances. Upper frame: The SBE profile is similar to the experimental one (see Figure 1). Middle frame: circles represent the averaged histogram of ΔISI histograms of all the simulated neurons. An averaged value is obtained for each time bin. The solid line is a computer generated Lévy histogram with $\alpha = 1.25$, $\gamma = 5$. Fits to the data followed the maximum likelihood method of (Nolan, 2000). The temporal resolution of spikes is set at 1msec. Lower frame: circles represent the histogram of the simulated ΔIEI time sequence. The solid line is a computer generated Lévy histogram ($\alpha = 1.6$, $\gamma = 25$). The temporal resolution of SBEs is 100msec.

5 Testing the model

5.1 Sensitivity to choice of parameters

To gain further understanding of the model we test its sensitivity to different parameters. The ratio of the number of excitatory to inhibitory neurons affects the rate and the shape of SBEs. Increasing the number of inhibitory neurons decreases the probability to generate SBEs. Moreover, strong inhibition decreases the activity of neurons during a SBE, resulting in a very dilute event. On the other hand, in the absence of inhibition (i.e. in an excitatory network) the network operates in an asynchronous mode, without generating SBEs. However, decreasing synaptic strengths 10-fold, the network reduces its total activity and SBEs appear. This effect was referred in (Tsodyks, Uziel & Markram, 1999). Reducing synaptic strengths further, the SBEs are still obtained but their profile becomes symmetric.

The synaptic strengths (or resistances) determine the shape of the distributions. When A_{ij} is reduced by the same factor for all synapses attached to a post-synaptic neuron, the activity during a SBE is less dense (small I_{syn}), and the density of SBEs is reduced. This results in an increase of both γ (the bending point) and α (the long-tail decay) of the Lévy distribution of ΔISI. The effect on the shape of the ΔIEI distribution is very weak. There is a limit to our ability to control the shape of the distributions. Reducing the synaptic strengths leads to low activity rate with symmetric SBEs and eventually to disappearance of SBEs. Increasing synaptic strengths leads to high activity rate, eventually obtaining merger of SBEs into a tonic firing mode.

The time constant of the dynamic thresholds τ_{th} provides further flexibility in adjusting ΔISI to experimental data. An example is shown in Figure 6 where we compare our model to a specific experiment, obtaining a good fit to

a Lévy distribution almost up to 1000msec. In fact, the increase of τ_{th} allowed us to increase the domain over which the Lévy distribution is valid from 100 to 1000msec.

5.2 Self-consistency

Using experimental data we can test the model. We feed a simulated neuron with spike sequences of the experimental neurons, via frequency-dependent synapses, while removing the external input. We have data of 36 real neurons and we label arbitrarily 32 of them as excitatory pre-synaptic neurons and 4 as inhibitory ones. We expect the simulated neuron to be synchronized with the network activity, i.e. to spike mainly within SBEs. The question to be tested is whether the distribution of its output spike train will match the experimental one (average of all experimental neurons). The results indicate that the model is consistent with the experimental activity: When a simulated neuron receives a Lévy distributed stimulus it responds with a Lévy distributed pattern of activity. The exact pattern is determined mainly by the choice of synaptic strengths. There are only slight differences between the response of an IF neuron with a fixed threshold and an IF neuron with a dynamic threshold given our set of parameters.

In some experimental preparations we notice that there are few neurons that have much higher firing rates than others. It would be interesting to find the character of these neurons. In particular to understand if they are inhibitory neurons, whose role is to regulate the activity of the network, or excitatory ones reacting to the changing environment. An experimental method to answer this question can be suggested on the basis of our model. The real neurons can be stimulated electrically through the electrode they are attached to. One can inject positive currents to one of the neurons, causing it to spike intensively.

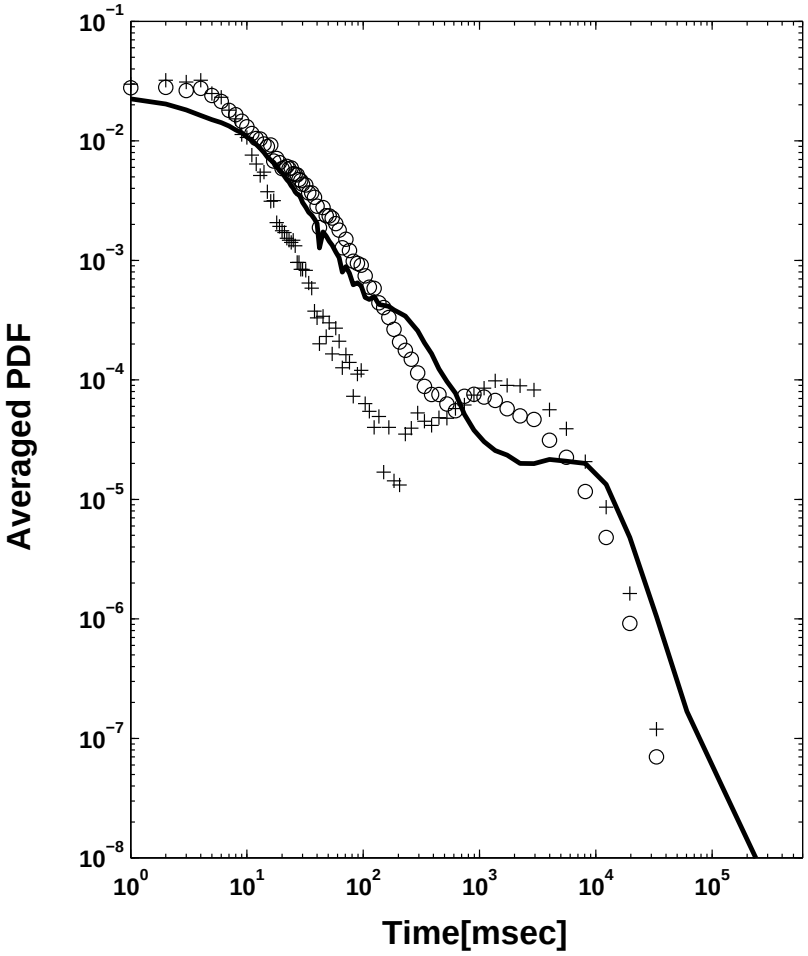

Figure 6: The effect of τ_{th} on the model for ΔISI. Solid curve: The averaged histogram of all the neurons of the experimental system (same data as in Figure 2). Symbols: Averaged histograms calculated for the results of the simulation. (+) curve $\tau_{th} = 100$msec. (o) curve: $\tau_{th} = 450$msec $\alpha \simeq 0.8$, $\gamma \simeq 20$. Note that τ_{th} affects mainly the slope of the histogram. The KL distance measure between these two models and the averaged experimental histogram are: $D_{KL}(+) = 9.5695 \cdot 10^{-6}, D_{KL}(o) = 2.5147 \cdot 10^{-7}$.

The specific balance in our simulated network enables a higher firing rate for inhibitory neurons than for excitatory neurons. This could be tested. Injecting an excitatory neuron with positive currents, thus making it permanently active, we find in our model that this is sufficient to induce permanent activity in any inhibitory neuron connected to that excitatory neuron, but not in any other excitatory neuron. This is demonstrated in Figure 7. It can be used as a basis for mapping out inhibitory neurons in the experimental preparation. It also suggests that the observed spiking neurons in the (unstimulated) preparation are inhibitory neurons whose activity may regulate the system.

6 Discussion

From the results of section 4 we conclude that inhomogeneities in neural parameters lead to correct behavior of the neuronal activity: 1. Time-varying external currents lead to the rising spatio-temporal profile of a SBE. 2. Inhomogeneity in the resistances leads to the detailed structure of a SBE. 3. The accurate distributions of spikes is obtained using dynamic thresholds. 4. A Lévy distribution of SBEs is also obtained due to inhomogeneity in the system.

Dynamic thresholds are often used to account for neuronal adaptation through their increase. In the model of section 4 we have employed two types of neurons, having both increasing and decreasing dynamical thresholds. This observation is consistent with known biological observations of a large firing repertoire of neurons (Meunier & Segev, 2001). Moreover, a recent study of inter-neurons (Markram, 2003) reported the existence of many types of inhibitory neurons, each having its own characteristic electrical response to stimulus.

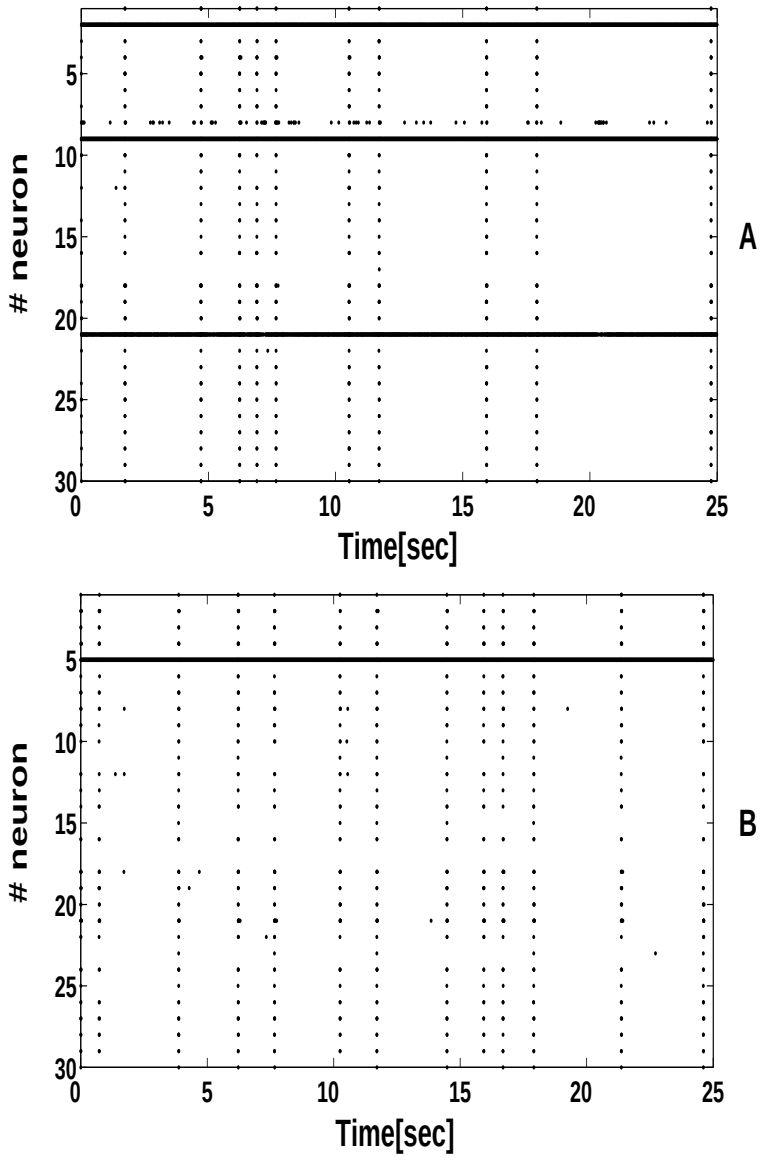

Figure 7: Response of the model to external stimulations. Upper frame: Positive external current is injected to an excitatory neuron (number 9). The target inhibitory neurons numbers 2 and 21 respond with continuous spiking. Target neuron number 8 is also inhibitory and shows extensive spiking outside SBEs. All the rest are excitatory neurons that spike only within SBEs. Lower frame: Positive external current is injected to an excitatory neuron (number 5) that does not have any inhibitory neurons as targets. Hence no other neurons exhibit continuous spiking behavior.

It has been suggested a long time ago (Gerstein & Mandelbrot, 1964) that if the membrane voltage has a random-walk behaviour, one can obtain many heavy-tailed distributions. Dynamic thresholds of the kind we use impose a random-walk-like behaviour on the membrane voltage, and were necessary to obtain the distributions observed experimentally, so our results embrace their suggestion. To reinforce this claim, we also examined non-linear one-dimensional models of neurons, which describe more accurately the changes in the membrane voltage. Using these models in the absence of dynamic thresholds did not lead to better results. However, using a two-dimensional model which endows its membrane with more complicated response by making partial use of ionic channel dynamics can explain the neuronal distributions we see in the experiments (Volman, Baruchi, Persi & Ben-Jacob, 2004).

The variance of the heavy-tailed distributions of ΔISI diverges. This may imply that the system we study has the potential to operate on many different time scales. This flexibility is important to allow different neuronal networks, with different functional roles, to be responsive to different time scales depending on the specific inputs they have to process. Therefore, in a case of processing a given task (or stimulation) we would expect to observe changes in the shape and variability of the discussed distributions. It will be interesting to understand which features of the stimulation will be coded by the individual neurons and which features (if any) will be coded on the whole network level. This will be tested in the future.

An important open problem is to understand why networks of different sizes behave similarly. We believe that this can be understood by invoking the concept of neural regulation (Horn, Levy & Ruppin, 1998) or synaptic scaling (Turrigiano et al., 1998; Abbott & Nelson, 2000). Preliminary studies show this to be the case, but it requires further investigation.

Acknowledgment

This work was supported by a research grant of the Israel Science Foundation.

Appendix

Parameters of simulation in (Tsodyks, Uziel & Markram, 1999): 400 excitatory neurons and 100 inhibitory neurons. Reset and threshold membrane potentials: $V_{reset} = 13.5$ and $V_{threshold} = 15$. Resistances are 1. External currents were driven from a unit distribution centered at the threshold level with a range of 5% of the threshold. Time constants of the neurons: $\tau_{mem} = 30$msec, refractory period of 2 and 3 msec for inhibitory and excitatory neurons, respectively. Synaptic parameters were taken from Gaussian distributions. Standard deviations are half of the following average values (with cutoffs of 2·average and 0.2·average): A(ee) = 1.8, A(ei) = 5.4, A(ie) = A(ii) = 7.2. Average values of utilization: U(ee) = U(ei) = 0.5, U(ie) = U(ii) = 0.04. Average time constants: τ_{rec}(ie) = τ_{rec}(ii) = 100msec, τ_{rec}(ee) = τ_{rec}(ei) = 800msec, τ_{fac}(ie) = τ_{fac}(ii) = 1000msec. Fixed time constant of $\tau_{ina} = 3$msec. It is reported that the results of this simulation are robust under changes of up to 50% in the average values.

Parameters of our model:

27 excitatory neurons and 3 inhibitory neurons. Reset and threshold membrane potentials: $V_{reset} = 0$ and $V_{threshold} = 1$. Resistances to synaptic currents $\sim$ U(0.1,0.4). Resistance to external currents remains 1. External currents $\sim$ N(0.86,0.15). Time constants of the neurons: $\tau_{mem} \sim$ U(9.5,10.5)msec, refractory periods $\sim$ U(2,3)msec for all neurons. Fixed time constant of $\tau_{ina} =$ 10msec. All other parameters are unchanged.

References

Abbott L.F. and Nelson Sacha B. (2000). Synaptic Plasticity: taming the beast. *Nature Neuroscience Supplement 3,* 1178-1183.

Brandman R. and Nelson Mark E. (2002). A simple model of long-term spike train regularization. *Neural Computation 14,* 1575-1597.

Gerstein G. and Mandelbrot B. (1964). Random walk models for the spike activity of single neuron. *biophysical Journal 4,* 41-68.

Horn D., Levy N. and Ruppin E. (1998). Memory maintenance via neuronal regulation. *Neural computation 10,* 1-18.

Horn D. and Opher I. (1999). Complex dynamics of neuronal thresholds. *CNS 99.*

Horn D., and Usher M. (1989). Neural Networks with Dynamical Thresholds, *Phys. Rev. A40,* 1036-1044.

Lowen S., Ozaki T., Kaplan E., Saleh B. and Teich M. (2000). Fractal features of dark, maintained and driven discharges in the cat visual system. *Methods: A Companion to Methods in Enzymology.*

Mantegna R.N. and Stanley H.E. (1995). Scaling behaviour in the dynamics of an economic index. *Nature 376,* 46-49.

Markram H. (2003). Molecular determinants of neuronal diversity. Lecture at the Brain in Motion symposium, EPFL Lausanne.

Markram H., Pikus D., Gupta A. and Tsodyks M. (1998). Potential for multiple mechanisms, phenomena and algorithms for synaptic plasticity at single synapses. *Neuropharmacology 37,* 489-500.

Markram H. and Tsodyks M. (1996). Redistribution of synaptic efficacy between neocortical pyramidal neurons. *Nature 382,* 807-810.

Marom S. and Shahaf G. (2002). Development, learning and memory in large random networks of cortical neurons: lessons beyond anatomy. *Quarterly*

Rev. of Biophysics 35, 63-87.

Meunier C. and Segev I. (2001). Neurons as physical objects: structure, dynamics and function. In handbook of biological physics, Vol. 4 *Elsevier,* 353-466.

Nolan J.P. (2000). Maximum likelihood estimation and diagnostics for stable distributions. In O.E. Barndorff-Nielsen, T. Mikosch, and S.I. Resnick (Eds.). *Lévy processes: Theory and Applications.*

Nolan J.P. (1998). Parameterization and modes of stable distribution. *Statistics and Probability Letters 38,* 187-195.

Nolan J.P. (2004). Stable distributions - models for heavy-tailed data. *in press, Boston: Birkhauser* chapter 1. available at: http: //academic2.american.edu/ jpnolan/

Peng C.K., Mietus J., Hausdorff J.M., Havlin S., Stanley H.E. and Goldberger A.L. (1993). Long-range anticorrelations and non-Gaussian behavior of the heartbeat. *Phys. Rev. Lett. 70,* 1343-1346.

Segev R. (2002). Self-organization of in vitro neuronal networks. *PhD Thesis, Tel-Aviv University.*

Segev R., Benveniste M., Shapira Y., Hulata E., Cohen N., Palevski A., Kapon E., and Ben-Jacob E. (2001a). Long-term behavior of lithographically prepared in vitro neural network. *Physical Review Lett. 88,* p.118102.

Segev R., Shapira Y., BenVeniste M. and Ben-Jacob E. (2001b). Observation and modeling of synchronized bursting in two-dimensional neural network *Physical Review E. 64,* p. 011920.

Shahaf G. and Marom S. (2001). Learning in networks of cortical neurons. *Journal of Neuroscience 21(22),* 8782-8788.

Tsodyks M., Pawelzik K. and Markram H. (1998). Neural networks with dynamic synapses. *Neural computation 10,* 821-835.

Tsodyks M., Uziel A. and Markram H. (1999). Synchrony generation in recurrent networks with frequency-dependent synapses. *Journal of Neuroscience 20,* RC50 1-5.

Turrigiano G., Leslie K., Desai N., Rutherford L. and Nelson S. (1998). Activity-dependent scaling of quantal amplitude in neocortical neurons. *Nature 391,* 892-895.

Volman V., Baruchi I., Persi E. and Ben-Jacob E. (2004). Generative modelling of regulated dynamical behavior in cultured neuronal networks *Physica A Vol 335,* 249-278.

Ying-Hui L. and Wang X.J. (2000). Spike-frequency adaptation of generalized leaky integrate and fire model neuron. *Journal of Computational Neuroscience 10,* 25-45.